# Eigenvector localization in hypergraphs: Pairwise versus higher-order links

Ankit Mishra [*] and Sarika Jalan [†]

*Department of Physics, Complex systems Lab, Indian Institute of Technology Indore, Khandwa Road, Simrol, Indore-453552, India*

(Received 5 September 2022; accepted 2 March 2023; published 22 March 2023)

Localization behaviors of Laplacian eigenvectors of complex networks furnish an explanation to various dynamical phenomena of the corresponding complex systems. We numerically examine roles of higher-order and pairwise links in driving eigenvector localization of hypergraphs Laplacians. We find that pairwise interactions can engender localization of eigenvectors corresponding to small eigenvalues for some cases, whereas higher-order interactions, even being much much less than the pairwise links, keep steering localization of the eigenvectors corresponding to larger eigenvalues for all the cases considered here. These results will be advantageous to comprehend dynamical phenomena, such as diffusion, and random walks on a range of real-world complex systems having higher-order interactions in better manner.

DOI: 10.1103/PhysRevE.107.034311

## I. INTRODUCTION

Network science has been a powerful means to construe and predict properties of many real-world complex systems [1–4]. A network consists of nodes, microscopic units of the underlying system, and links which represent interactions among the nodes. Many real-world complex systems inherently share common structural properties, such as power-law degree distributions, short path lengths, high clustering, degree-degree correlation, etc. These structural properties govern various dynamical processes on networks, for instance, disease spreading [5], steady-state behaviors of random walkers [6], synchronization [7], etc. Despite an astounding theoretical success of the network theory in comprehending properties of the associated complex systems, it often becomes insufficient to fathom origin behind many emerging dynamical behaviors of many real-world complex systems. With the increasing accumulation of data, it has been construed that often real-world interactions transpire among more than two nodes at a time, whereas, the network theory is apt for the binary relationships between nodes [8]. The inefficacy of networks to model many-body interactions compelled researchers to look beyond the realm of pairwise interactions and develop appropriate higher-order models. The two most popular approaches for modeling higher-order interactions are hypergraphs [9] and simplicial complexes [10].

Hypergraphs capturing higher-order interactions provide a more generalized model for real-world complex systems. A hypergraph consists of nodes and hyperedges; a hyperedge connects $d$ nodes together where typically $d \geqslant 2$. The size of the hyperedges of a hypergraph may differ. Nevertheless, if all the hyperedges consist of the same number of nodes $d$, it is referred to as a $d$-uniform hypergraph. Thus, a two-uniform hypergraph would correspond to a conventional graph. Hypergraphs have been successfully employed to illustrate various real-world interactions from biology [11], social systems [12], evolutionary dynamics [13], etc. A simplicial complex is a special type of hypergraph, which is closed under the subset operation [14,15]. A simplicial complex not only is comprised of nodes and links, but also corroborates higher-order dimensions, such as triangles, tetrahedrons, etc. Accordingly, a $k$ simplex describes a simultaneous interactions among $k+1$ nodes A fundamental difference between modeling many-body interactions with the hypergraphs and simplicial complexes is that a $k$ simplex subsumes all the possible $k-1$ dimension simplices, which is not true with the former.

Moreover, the spectra of adjacency and Laplacian matrices are recognized to affect various dynamical processes on corresponding networks. For example, an epidemic threshold of the infection rate on graphs is determined by the inverse of the principal eigenvalue of the associated adjacency matrices [16]. Furthermore, under appropriate conditions, the critical coupling strength at which synchronization occurs in coupled oscillators on networks is determined by the largest eigenvalue of the adjacency matrices [17]. Spectra of the adjacency matrix also furnish insight into various structural properties of corresponding complex networks [18–21]. Likewise, spectra of the Laplacian matrices are related to the diffusion and other spreading phenomena on networks [22]. Withal, spectral dimension supplies a mean to characterize or determine the return probability of diffusion [23], scaling of return time of a random walker for a magnetic model on graphs [24], return to the origin probability of the Gaussian model [25]. The ratio of the largest to the first nonzero eigenvalue of a Laplacian matrix helps in determining the stability of generalized synchronization in the coupled dynamical system [26]. Furthermore, Refs. [27], highlight the existence of relationships among topological, spectral, and dynamical properties of networks. In addition to the eigenvalues, eigenvectors of the underlying adjacency and the Laplacian matrices have also been indicated to be advantageous in

[*] ankitphy0592@gmail.com
[†] sarika@iiti.ac.in

 

providing insight into various structural and dynamical properties of the corresponding systems [28,29]. In particular, localization of eigenvectors ascribes crucially with disease spreading [30], perturbation propagation in ecological networks, [31], etc. Furthermore, analyzing localization properties of the Laplacian eigenvectors is advantageous in characterizing or identifying community structures [32], stability of the system against external shocks [33], network-turning patterns [34], etc.

Although a huge amount of literature on spectra of networks prevails, specifically, on eigenvector localization and their implications, an attempt has been made to comprehend localization properties of eigenvectors of the higher-order interaction graphs here. Here, we investigate localization properties of eigenvectors of hypergraphs comprising the higher-order interactions indicated by the hyperedges. We inspect hypergraphs instead of simplicial complexes as the latter involves complicated combinatorics, and, thus, the applications are limited to the lower dimension simplicial complexes, such as triangles and tetrahedrons [35]. On the other hand, in the case of the hypergraphs, the information of higher-order structures is installed in a matrix form with the dimension equal to $NN$ where $N$ is the number of nodes. Furthermore, hypergraphs allow handling heterogeneous sizes of the hyperedges more efficiently than that of the simplicial complexes. Of late, works on hypergraphs include random walks [35,36], synchronization [37–39], social contagions [14,40], evolutionary dynamics [13], etc. Most of these works, spotlighting on hypergraphs, converges on projecting hypergraphs into their weighted pairwise networks and, thereupon comparing various structural and dynamical properties between the hypergraphs and the projected pairwise networks. In this paper, we take a slightly different approach, and instead of projecting a hypergraph into a corresponding pairwise network, we consider contributions from the higher-order and pairwise interactions for each node. Thereafter, by defining parameter $\gamma$, we compare the relative contributions of these two types of interactions in the steering localization of the eigenvectors of hypergraph Laplacians. We find that eigenvectors are localized on those nodes which have their pairwise or higher-order degrees considerably deviating from the average pairwise degree ($\langle k^p \rangle$) and average higher-order degree ($\langle k^h \rangle$) of the hypergraph, respectively.

The paper is organized as follows. Section II comprises definitions of the Laplacian matrices of hypergraphs. Section III introduces the hypergraph model. Section IV discusses the methodology and techniques involved in the paper. Section V contains results about significance of the interplay of pairwise and higher-order links on eigenvector localization. Finally, Sec. VI concludes the paper with future directions.

## II. LAPLACIAN MATRIX

A hypergraph denoted by $H = \{V,\ E^H\}$ consists of a set of *nodes* and *hyperedges*. The set of *nodes* is represented by $V = \{v_1\text{–}v_3,..., v_N\}$, and the set of *hyperedges* is represented by $E^H = \{E_1\text{–}E_3,..., E_M\}$ where $N$ and $M$ are the sizes of $V$ and $E^H$, respectively. Note that, each hyperedge $E_\alpha$, $\forall\, \alpha = 1, 2,..., M$, will contain a collection of nodes, i.e., $E_\alpha \subset V$. Thus, when $|E_\alpha| = 2$ for all $\alpha$'s, the hypergraph reduces to a standard graph. Mathematically, a hypergraph can be represented by its incidence matrix $(e_{i\alpha})_{NM}$ whose elements are defined as

$$e_{i\alpha} = \begin{cases} 1, & v_i \in E_\alpha, \\ 0, & \text{otherwise.} \end{cases} \tag{1}$$

One can easily build the $NN$ adjacency matrix for a hypergraph using Eq. (1), as $A = ee^T$. The entries of the adjacency matrix $A_{ij}$ represents the number of hyperedges containing both $i$ and $j$ nodes. It is important to note here that the adjacency matrix is often obtained by setting 0 to its diagonal entries. We further define $MM$ hyperedges matrix $C = e^T e$, whose the entry $C_{\alpha\beta}$ represents the number of nodes common between the hyperedges $E_\alpha$ and $E_\beta$.

There exists no unique way to define the Laplacian matrix $L$ of a hypergraph [8]. One of the conventional manners is as follows; $L_{ij} = k_i\delta_{ij} - A_{ij}$ where $k_i = \sum_{j=1}^{N} A_{ij}$ denotes the number of hyperedges containing node $i$. However, it is not consistent with the full higher-order structures encrypted in the hypergraph. More specifically, it does not account for the sizes of the hyperedges incident on a node. Reference [35] solved this limitation by defining a new Laplacian matrix for a random walk, which is also consistent with the higher-order structures. The transition probability of a random walker defined in Ref. [35] takes care of the size of the hyperedges involved. More precisely, the Laplacian of the random walk (RW) defined in Ref. [35] is as follows:

$$L^{\mathrm{RW}}_{ij} = \delta_{ij} - \frac{k^H_{ij}}{\sum_{i\neq\ell} k^H_{i\ell}}, \tag{2}$$

and the entries of the $K^H$ matrix are given by

$$k^H_{ij} = \sum_{\alpha}(C_{\alpha\alpha} - 1)e_{i\alpha}e_{j\alpha} = (e\hat{C}e^T)_{ij} - A_{ij}, \quad \forall\, i \neq j, \tag{3}$$

where $\hat{C}$ is a matrix whose diagonal entries coincide with that of $C$ and other entries are *zero*. Using Eqs. (2) and (3) [36], we construct the combinatorial Laplacian matrix for the hypergraph, given by

$$L^H = K^H - D. \tag{4}$$

Here, $D$ is a diagonal matrix whose entries are $D_{ii} = k^H_i = \sum_{i\neq\ell} k^H_{i\ell}$, and *zero* otherwise. Note that, in accordance with the earlier convention, i.e., setting 0 to the main diagonal, $k_{ii} = 0$. The Laplacian matrix is defined by Eq. (4) which takes into account both the number and the size of the hyperedges incident on the nodes, and, thus, incorporates the higher-order structures completely. By considering $L^H$ as a Laplacian of the hypergraph, here we study the effect of higher-order structures on steering the eigenvector localization.

## III. MODEL

There are various manners in which a random hypergraph can be constructed [8]. We generate the hypergraph in this paper as follows. Starting from a ring lattice in which each node is connected to its nearest neighbors on both the sides, we randomly choose $d$ nodes uniformly from all the existing nodes. If there exists no hyperedge comprising of the chosen $d$ nodes, we add a hyperedge consisting of these $d$ nodes. For

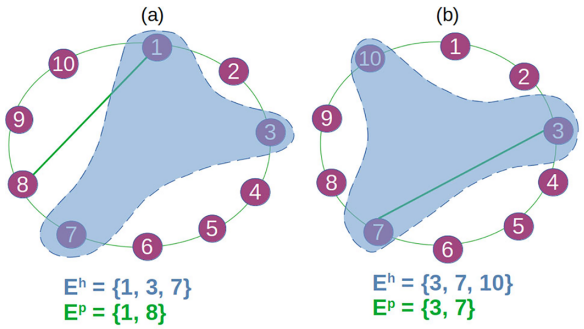


FIG. 1. Schematic of the hypergraph model used here with $N = 10$, $M^h = 1$, and $M^p = 1$ for two different realizations. (a) *One* pairwise link $E^p = \{1, 8\}$ and *one* hyperedge $E^h = \{1, 3, 7\}$ are added into the ring lattice. (b) *One* pairwise link $E^p = \{3, 7\}$ and *one* hyperedge $E^h = \{3, 7, 10\}$ are added into the ring lattice. The pairwise links are solid lines (green) and the hyperedge with the dashed line (sky-blue) enclosing the involved nodes.

the simplicity, we consider $d = 3$ for each iteration. Next, we add pairwise links by choosing $d = 2$ nodes uniformly and randomly from the existing nodes. The pairwise links are added to the model so that an interplay of the higher-order and pairwise links on the eigenvector localization can be investigated. Figure 1 presents a schematic of the model for two different cases; (a) no pairwise links exists between nodes involved in a hyperedge and (b) pairwise links exist in the nodes belonging to the hyperedge. Note that, a similar model was also used in Ref. [41], but no pairwise links were added to the original ring lattice. We would like to further mention here that one can choose an alternate algorithm to generate the given model as introduced in Ref. [42]. In the alternate approach, for each node, one can choose *two* other nodes with a probability $p$, and add hyperedges containing the nodes under consideration. Similarly, one can add pairwise links by associating *one* node for a given node. Thus, the total number of the hyperedges, and pairwise links each will be equal to $pN$. However, in one loop only $N$ pairwise links can be added for $p = 1$. To add more pairwise links, one has to again repeat the entire algorithm. Hence, we use the former algorithm in which the number of pairwise links and hyperedges are admitted from the beginning.

## IV. METHODS

As discussed earlier, a hypergraph can be represented by its Laplacian matrix $L^H$. Let the eigenvalues of the Laplacian matrix denoted by $\{\lambda_1\text{–}\lambda_3, \ldots, \lambda_N\}$ where $\lambda_1 \geqslant \lambda_2 \geqslant \cdots \geqslant \lambda_N$ and the corresponding orthonormal eigenvectors as $\{\boldsymbol{x}_1\text{–}\boldsymbol{x}_3, \ldots, \boldsymbol{x}_N\}$. The Laplacian matrix is positive semidefinite, i.e., $\sum_{i,j} L^H_{i,j} x_i x_j \geqslant 0$ for any vector $\boldsymbol{x} = (x_1\text{–}x_3, \ldots, x_N)$. Therefore, all the eigenvalues of the Laplacian matrix are positive with one and only one being zero for the connected network. The entries of the eigenvector corresponding to this *zero* eigenvalue will be uniformly distributed $(1, 1, \ldots, 1)/\sqrt{N}$. The generalized degree of a node $i$ in the hypergraph is given by $k^H_i$ which can be further decomposed into $k^H_i = k^h_i + k^p_i$ where $k^h_i$ and $k^p_i$ are the contributions from the higher-order and the pairwise links, respectively. Similarly, the average degree, $\langle k \rangle = \frac{\sum_i k^H_i}{N}$, can be decomposed as $\langle k \rangle = \langle k^h \rangle + \langle k^p \rangle$ where $\langle k^h \rangle = \frac{\sum_i k^h_i}{N}$ and $\langle k^p \rangle = \frac{\sum_i k^p_i}{N}$. We would like to further define $\langle k \rangle$ in terms of total number of the higher-order and pairwise links as $\langle k \rangle = \frac{2M^p}{N} + \frac{12M^h}{N}$, where $M^p$ and $M^h$ are total numbers of the pairwise edges ($d = 2$) and the hyperedges ($d = 3$) in the hypergraph. Also, it is important to note that if a node, say $i$, gets one additional pairwise link and one higher-order link, its degree will be increased by 1 and 4 from the pairwise and higher-order links, respectively. For example, if we consider the hypergraph depicted in Fig. 1(a), the first row of the $K^H$ matrix ($i = 1$) is the following: $k^H_{1j} = [0, 1, 2, 0, 0, 0, 2, 1, 0, 1]$. Note that, $k^H_{13} = 2, k^H_{17} = 2$ from the hyperedge. Therefore, $k^H_1 = 7$ with $k^h_1 = 4$ and $k^p_1 = 3$. Hence, $k^h_i = 4M^h_i$, where $M^h_i$ is the total number of higher-order links incident on node $i$. To provide an equal opportunity to the pairwise and higher-order links for steering localization on a given node, we introduce the total number of pairwise links four times greater than the higher-order links, i.e., $M^p = 4M^h$ for $k^h_i = k^p_i$. Next, we define a parameter $\gamma = \frac{M^p}{4M^h}$ to measure the relative contribution for both types of the links. Thus, if $\gamma > 1$ then $k^p_i > k^h_i$; if $\gamma < 1$ then $k^p_i < k^h_i$ holds.

We examine the localization property of the eigenvectors of the hypergraph, and analyze the changes in the localization behavior as the pairwise and the higher-order links are introduced on the initial ring lattice. Localization of an eigenvector refers to a state that a few entries of the eigenvector acquire much higher values compared to the others. Degree of localization of the $\boldsymbol{x}_j$th eigenvector can be quantified by measuring the inverse participation ratio (IPR) denoted as $Y_{\boldsymbol{x}_j}$. The IPR of an eigenvector $\boldsymbol{x}_j$ is defined as [30]

$$Y_{\boldsymbol{x}_j} = \sum_{i=1}^{N} (x_i)^4_j, \tag{5}$$

where $(x_i)_j$ is the $i$th component of the normalized eigenvector $\boldsymbol{x}_j$ with $j \in \{1\text{–}3 \ldots, N\}$. One can easily verify that, for the most delocalized eigenvector all its components should be equal, i.e., $(x_i)_j = \frac{1}{\sqrt{N}}$ with the IPR value being $1/N$. Whereas, for the most localized eigenvector, only one component of the eigenvector will be nonzero, and, consequently, IPR will be equal to 1. It is also important to note here that there may exist fluctuations in the IPR values for a given state $\boldsymbol{x}_j$ for different realizations. However, it is not possible that $\lambda_j$ remains the same for all the random realizations, and, hence, averaging over should be performed diligently. For the robustness of the results, we consider a small width $d\lambda$ around $\lambda$, and average all the IPR values corresponding to those $\lambda$ values which fall inside this small width. Thus, we present results for average over small width $d\lambda$, which is indeed a general practice in the localization studies [43–45]. We further elaborate on the averaging procedure for the discrete eigenvalues spectrum achieved through the numerical calculations. Let $\lambda^R = \{\lambda_1, \lambda_2, \ldots, \lambda_{NR}\}$ such that $\lambda_1 \leqslant \lambda_2 \leqslant \cdots \leqslant \lambda_{NR}$ is a set of eigenvalues of the hypergraph for all $R$ random realizations where $NR$ is the size of $\lambda^R$. The corresponding eigenvector of $\lambda^R$ is denoted by $\boldsymbol{x}^R = \{\boldsymbol{x}_1\text{–}\boldsymbol{x}_3, \ldots, \boldsymbol{x}_{NR}\}$. We then divide $\lambda^R$ for a given value of $d\lambda$ into further $m$ subsets where $m$

$= (\lambda_{NR} - \lambda_1)/d\lambda$. For each $\lambda^j \subset \lambda^R$ and the corresponding eigenvectors $\boldsymbol{x}^j \subset \boldsymbol{x}^R$, $\forall\, j = 1, 2, ..., m$; $\lambda^j = \{\lambda_1, \lambda_2, ..., \lambda_{l^j}\}$ and corresponding eigenvector $\boldsymbol{x}^j = \{\boldsymbol{x}_1 \text{–} \boldsymbol{x}_3, \ldots, \boldsymbol{x}_{l^j}\}$ where $l^j$ is the size of the $j$th subset such that $\sum_{j=1}^{m} l^j = NR$ with a constraint that $\lambda_{l^j} - \lambda_{1^j} \leqslant d\lambda$. For each subset, the corresponding set of IPRs for $\boldsymbol{x}^j$ will be $\{Y_{\boldsymbol{x}_1}, Y_{\boldsymbol{x}_2}, ..., Y_{\boldsymbol{x}_{l^j}}\}$. Hence, the average IPR $[Y_{\boldsymbol{x}_j}(\lambda)]$ for each subset $\boldsymbol{x}^j$ can be calculated as $\frac{\sum_{i=1}^{l^j} Y_{\boldsymbol{x}_i}}{l^j}$ where $\lambda$ is the central value for each subset, i.e., $\lambda + \frac{d\lambda}{2} = \lambda_{l^j}$ and $\lambda - \frac{d\lambda}{2} = \lambda_{1^j}$. Here, we define few more physical quantities, $k^h(\lambda)$, $k^p(\lambda)$, $\hat{k}^h(\lambda)$, and $\hat{k}^p(\lambda)$ used in the paper. For any eigenvector $\boldsymbol{x}_j$, these quantities can be calculated as the following.

$k^h_{\boldsymbol{x}_j}$: higher-order degree of the node $i_o$ with the maximum component in $|(x_i)_j|$, i.e., $(x_{io})_j = \max\{|(x_1)_j|, |(x_2)_j|, \ldots, |(x_N)_j|\}$.

$k^p_{\boldsymbol{x}_j}$: pairwise degree of the node $i_o$ with the maximum component in $|(x_i)_j|$, i.e., $(x_{io})_j = \max\{|(x_1)_j|, |(x_2)_j|, \ldots, |(x_N)_j|\}$.

$\hat{k}^h_{\boldsymbol{x}_j}$: higher-order degree expectation value of eigenvector, defined as $\sum_{i=1}^{N} (x_i)_j^2 k_i^h$.

$\hat{k}^p_{\boldsymbol{x}_j}$: pairwise degree expectation value of eigenvector, defined as $\sum_{i=1}^{N} (x_i)_j^2 k_i^p$.

All these physical quantities obey the same averaging procedures over $\lambda$ and $\lambda \pm d\lambda$ as described for IPR, and we obtain $k^h(\lambda)$, $k^p(\lambda)$, $\hat{k}^h(\lambda)$, and $\hat{k}^p(\lambda)$.

## V. RESULTS

We first discuss the degree-eigenvalue correlation of the Laplacian of the hypergraphs. It was contemplated for pairwise interactions [46,47] that the eigenvalues of the Laplacian matrices have similar distributions as that of the degree of the nodes. The relative average deviation between the eigenvalues and degrees of a network can be defined as $\|\lambda(L) - k\|_2/\|k\|_2 \leqslant \sqrt{\|k\|_1/\|k\|_2^2}$, where $\lambda(L) = (\lambda_1, \lambda_2, \ldots, \lambda_N)^T$ and $k = (k_1, k_2, \ldots, k_N)^T$ are the eigenvalues of the Laplacian matrix and node degrees arranged in increasing order, respectively. The relative average deviation estimates, on average, that how much eigenvalues differ from the corresponding degrees and the proof of the inequality can be found in Ref. [46]. The $\|y\|_p$ represents the $p$ norms of any vector $y = (y_1, y_2, \ldots, y_n)$ and is defined as $(\sum_i |y_i|^p)^{1/p}$. Thus, we see that $\sqrt{\|k\|_1/\|k\|_2^2} \ll 1$, which implies that eigenvalue distribution and degree distribution will have similar natures. Also, it is well known that $\langle k \rangle = \langle \lambda \rangle$. Figure 2 plots the eigenvalues ($\lambda_i$) and degree ($k_i^H$) of the hypergraph arranged in an increasing order with $N = 2000$ and 40 random realizations for various $\gamma$ values. A clear degree-eigenvalue correlation can be a witness akin to the pairwise networks from Fig. 2.

Next, it is difficult to decompose an eigenvalue $\lambda_i$ exactly into $\lambda_i^h + \lambda_i^p = f(k_i^h) + f(k_i^h)$ parts as practiced for the node degree. Nevertheless, we can contemplate a few heuristic arguments as follows. First, we define $\delta_i^h = \frac{(|\lambda_i - k_i^h|)}{\lambda_i}$ and $\delta_i^p = \frac{(|\lambda_i - k_i^p|)}{\lambda_i}$ to analyze the relative deviations of the eigenvalues

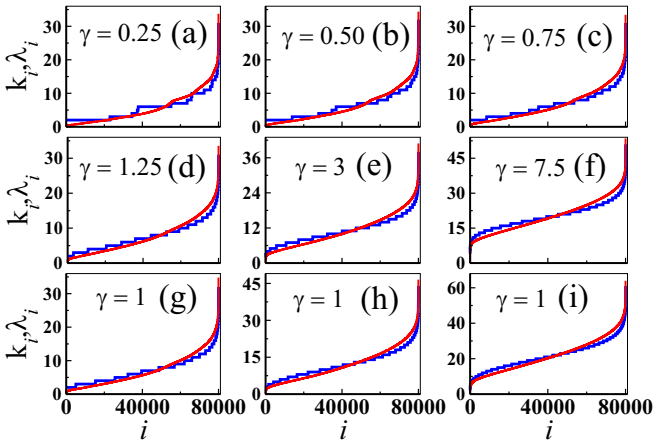


FIG. 2. Laplacian eigenvalues $\lambda_i$ (red) and node degree $k_i$ (blue) against index $i$ arranged in an increasing order for the $\gamma$ values. The size of the hypergraphs $N = 2000$ and $M^h = 500$ remain fixed for all $\gamma$ values with 40 random realizations.

from the higher-order and pairwise degrees. Figure 3 illustrates $\delta_i^h$, $\delta_i^p$ against $i$ for various $\gamma$ values. For $\gamma \leqslant 1$, for the initial eigenvalues ($\lambda \leqslant 6$) and index ($i \leqslant 40\,000$), $\delta_i^h > \delta_i^p$. Thus, the eigenvalues are more correlated with the pairwise degree than that of the higher-order degree. Thus, $\lambda_i^h < \lambda_i^p$ and also $k_i^h = 0$ for $i < 40\,000$ (not shown). For the intermediate eigenvalues $\delta_i^h \approx \delta_i^p$ and, thus, $\lambda_i^h \approx \lambda_i^p$. For the extremal eigenvalues and large indices, we see that $\delta_i^h \ll \delta_i^p$ and, therefore, $\lambda_i^p \ll \lambda_i^h$. We further mention here that for the said parameter, i.e., $\gamma < 1$, $M^h = 500$, $k^p_{\max} = 10$, and $k^h_{\max} = 24$, and, therefore, for the extremal eigenvalues, the higher-order degrees play a governing role. For $1 < \gamma \leqslant 3$, $\delta_i^h < \delta_i^p$ for the extremal eigenvalues since $k^p_{\max} < k^h_{\max}$ for $1 < \gamma \leqslant 3$. However, for $\gamma > 3$, $\delta_i^h > \delta_i^p$, and, thus, $\lambda_i^h < \lambda_i^p$ for entire eigenvalue spectrum. Next, we discuss the interplay of higher-order and pairwise links on instigating localization.

*For* $\gamma < 1$. We would first like to emphasize here that by merely calculating the IPR value of an eigenvector, one

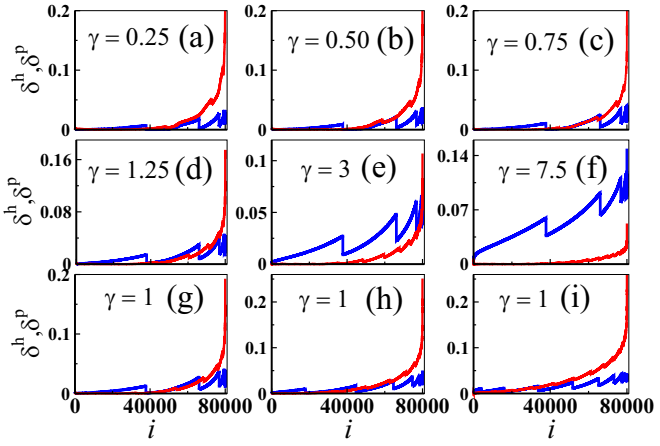


FIG. 3. The relative deviations of eigenvalues from the higher-order degrees, $\delta_i^h$ (blue) and pairwise degrees, $\delta_i^p$ (red) against index $i$. The hypergraph parameters, $N = 2000$ and $M^h = 500$, remain fixed for all $\gamma$ values with 40 random realizations.

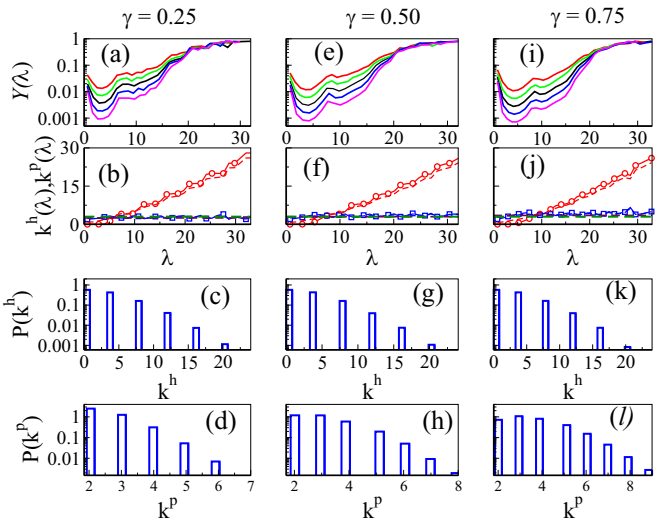


FIG. 4. Average IPR $[Y_{\boldsymbol{x}_j}(\lambda)]$, $k^h(\lambda)$ (○), $k^p(\lambda)$ (□), $\hat{k}^h(\lambda)$ (– – –), $\hat{k}^p(\lambda)$ (– – –) against $\lambda$ for various $\gamma < 1$'s. The corresponding higher-order and pairwise degree distribution are also plotted in last two rows. – – – and – · – · – depict, respectively, $\langle k^h \rangle$ and $\langle k^p \rangle$ on the $y$ axis. The size of the hypergraphs $N = 2000$ and $M^h = 500$ remain fixed for all $\gamma$ values with 40 random realizations for the bottom *three* rows. Red (–), green (–), black (–), blue (–), magenta (–) are used for $N = 500$, 1000, 2000, 4000, and 8000, respectively, in the upper panels.

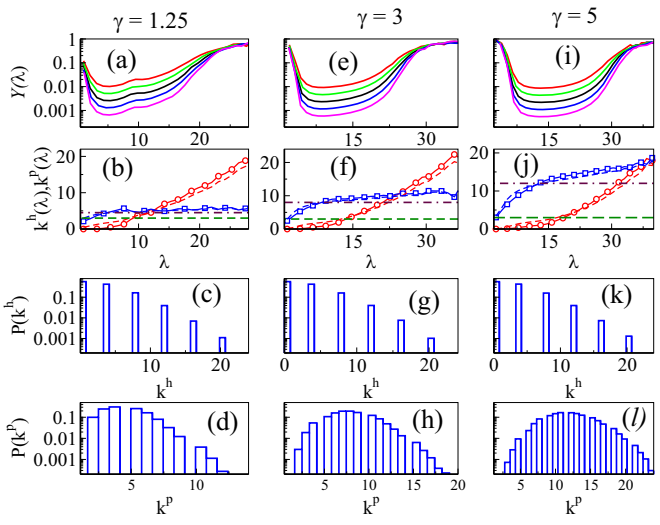


FIG. 5. Average IPR $[Y_{\boldsymbol{x}_j}(\lambda)]$, $k^h(\lambda)$ (○), $k^p(\lambda)$ (□), $\hat{k}^h(\lambda)$ (– – –), and $\hat{k}^p(\lambda)$ (– – –) against $\lambda$ for various $\gamma > 1$'s. The corresponding higher-order and pairwise degree distributions are also plotted in last two rows. – – – and – · – · – are at $\langle k^h \rangle$ and $\langle k^p \rangle$ on the $y$ axis. The size of the hypergraph, $N = 2000$ and $M^h = 500$ remain fixed for all $\gamma$ values with 40 random realizations for bottom *three* rows. Red (–), green (–), black (–), blue (–), and magenta (–) are used for $N = 500$, 1000, 2000, 4000, and 8000, respectively, in the upper panels.

cannot validate if the eigenvector is localized or delocalized as a critical phenomenon is accurately determined only for $N \to \infty$. To substantiate the localization behavior more precisely, one should check the scaling of the IPR with the system size. In general, $Y_{\boldsymbol{x}_j}(\lambda) \propto N^{-\alpha}$ with $\alpha = 0$ and 1 for localized and delocalized eigenvectors, respectively. For $0 < \alpha < 1$, the eigenvector can be referred to be at the critical state, i.e., neither localized nor delocalized. Figures 4(a), 4(e) and 4(i) present results for $Y_{\boldsymbol{x}_j}(\lambda)$ for different network sizes against $\lambda$ for various values of $\gamma < 1$. The larger eigenvalues in the eigenvalue spectrum ($\lambda > 22$) are localized with $Y_{\boldsymbol{x}_j}(\lambda) \to 1$ for all $N$'s and, thus, $\alpha = 0$. For $\lambda \leqslant 22$, eigenvalues are relatively less localized as compared with the larger eigenvalues, which can be verified by performing log-log curve fitting of $Y_{\boldsymbol{x}_j}(\lambda) \propto N^{-\alpha}$ and calculating $\alpha$ [Figs. 6(a)–6(c)]. It is apparent from the figure that according to the inclination towards localization or delocalization, $\alpha$ takes values accordingly. It is also worth mentioning here that there exists no noticeable change in the nature of the plot with an increase in $\gamma$, depicting the inefficacy of the pairwise links on instigating localization. Next, as reflected from Figs. 4(b), 4(f) and 4(j) that $k^p(\lambda)$ remains constant to a value around $\langle k^p \rangle$ for all the $\gamma$ values. Furthermore, Ref. [43] argued that localization of a eigenvector is centered on the nodes having very high or low degrees or whose degree deviate significantly from the average degree of the corresponding network. One can also note that for a completely delocalized eigenvector, degree expectation value $\hat{k} = \sum_{i=1}^{N} (x_i)_j^2 k_i = \frac{(k_1+k_2+k_3\cdots+k_N)}{N} = \langle k \rangle$. However, upon scrutinizing $k^h(\lambda)$ closely, we find that the its behavior is significantly different from $k^p(\lambda)$. $k^h(\lambda)$ exhibits an increasing trend with the increase in the eigenvalue, and takes the maximum possible value in the localized region. Thus, the eigenvectors are localized on the set of the nodes with $k^h$ being significantly higher than $\langle k^h \rangle$. Furthermore, in the same plot, $k^h(\lambda)$ and $k^p(\lambda)$ are shown to be in good approximation with the $\hat{k}^h(\lambda)$ and $\hat{k}^p(\lambda)$ values, respectively. Also, we plot the higher-order degree distribution $P(k^h)$ and pairwise degree distribution $P(k^p)$ in Figs. 4(c), 4(d), 4(g), 4(h), 4(k) and 4(l). Few interesting observations are as follows: The number of nodes with $k^h > 16$, $k^h > 12$, and $k^h > 8$ are only 0.04%, 0.64%, and 4%, respectively, and still the eigenvectors are localized on these nodes in the localized region. All these

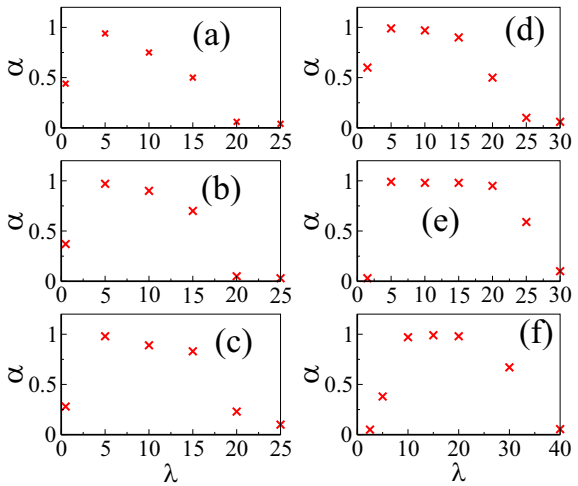


FIG. 6. Plot of $\alpha$ against $\lambda$ for various $\gamma$ values. (a) $\gamma = 0.25$, (b) $\gamma = 0.50$, (c) $\gamma = 0.75$, (d) $\gamma = 1.25$, (e) $\gamma = 3$, and (f) $\gamma = 5$.

observations clearly suggest prime role of the higher-order degree on instigating localization, and rather no visible impact of pairwise links on the same. Note that for $\gamma = 1$, there exists no sharp transition in the eigenvector localization and, thus, the next section focuses on $\gamma > 1$. The results for $\gamma = 1$ can be found in the Supplemental Material [48].

*For* $\gamma > 1$. Here, we discuss the localization properties of the eigenvectors for $\gamma > 1$. Figures 5(a), 5(e) and 5(i) present the results for $Y_{\boldsymbol{x}_j}(\lambda)$ for different network sizes as a function of $\lambda$ for various values of $\gamma > 1$. The extremal part of the eigenvalue spectrum (larger and smaller eigenvalues) are highly localized with $Y_{\boldsymbol{x}_j}(\lambda) \to 1$. On the contrary, the central part of the eigenvalue spectrum are delocalized with $10^{-3} \leqslant Y_{\boldsymbol{x}_j}(\lambda) < 10^{-2}$. Figures 6(d), 6(e) and 6(f) illustrates the behavior of $\alpha$ for different parts of the eigenvalue spectrum. In the localized part of the eigenvalue spectrum, $\alpha \approx 0$ whereas for the delocalized regime $\alpha \approx 1$. Furthermore, in accordance with the tendency towards localization or delocalization, $\alpha$ takes suitable values for other parts of the eigenvalue spectrum. Also, as $\gamma$ increases, the eigenvectors corresponding to the smaller eigenvalues get more localized captured by the IPR value. The nature of the plots is similar to those of the small-world networks (pairwise) shown in Ref. [43]. Furthermore, we report that the eigenvectors are localized on the nodes with degree ($k_i^H$) being abnormally high or low from the average degree ($\langle k \rangle$), which is consistent with the observations made in Refs. [43,49].

Next, we discuss the role of pairwise ($k_i^p$) and higher-order links ($k_i^h$) separately on steering the localization. Figs. 5(b), 5(f), and 5(j) illustrate the results for $k^h(\lambda)$, $k^p(\lambda)$, $\hat{k}^h(\lambda)$, and $\hat{k}^p(\lambda)$ for various $\gamma$ values. For $\gamma = 1.25$, $k^p(\lambda)$ remains constant around $\langle k^p \rangle$ but deviates slightly at the extremal parts of the eigenvalue spectrum. On the contrary, $k^h(\lambda)$ manifests an increasing trend with the increase in the eigenvalues and achieves large possible values in the localized region of the spectrum. As $\gamma$ increases, the pairwise links also start playing the role in steering the localization. First, the degree of localization of the eigenvectors corresponding to the smaller eigenvalues enhances. This can be explained as follows. For the case of smaller eigenvalues $k^h(\lambda)$ and $k^p(\lambda)$ both take very small values. However, as $\gamma$ increases the number of pairwise links also increases which, in turn, leads to an increase in $\langle k^p \rangle$. As discussed earlier that eigenvectors get localized on the nodes whose degrees deviate from the average degree. Thus, as $\gamma$ increases, $k^p(\lambda) \ll \langle k^p \rangle$ for smaller eigenvalues, which, consequently, intensifies the degree of localization. On contrary, $\langle k^h \rangle = 3$ remains fixed for all $\gamma$ values and, therefore, $k^h(\lambda)$ for smaller eigenvalues can not be much less than $\langle k^h \rangle$, therefore, suggesting no visible role of higher-order links in steering localization for smaller eigenvalues.

Next, we discuss the localization properties of the eigenvectors corresponding to those large eigenvalues, which are highly localized. From Figs. 5(b), 5(f) and 5(j), it is visible that for $\gamma \geqslant 3$, $k^p(\lambda)$ start deviating from $\langle k^p \rangle$, and, hence, the pairwise links also start participating in instigating localization along with the higher-order links. Few interesting things to be noted here are as follows: The number of nodes with large $k^h$ values are always very less as compared to the number of nodes with large $k^p$ values for $\gamma \geqslant 3$ [Figs. 5(c), 5(g) and 5(k)]. Scrutinizing more closely, we witness that the number of nodes with $k^h > 8$, $k^h > 12$, $k^h > 16$, and $k^h > 20$ are roughly around 4%, 0.73%, 0.11%, and 0.06%, respectively, for all $\gamma$ values. On the other hand. For $\gamma = 3$, the number of nodes with $k^p > 8$ and $k^p > 12$ are 39% and 4.27%, respectively. For $\gamma = 5$, the number of nodes with $k^p > 12$ and $k^p > 16$ are 41% and 8%, respectively. For $\gamma = 7.5$, the number of nodes with $k^p > 16$ and $k^p > 20$ are 53% and 18%, respectively. Therefore, despite the number of nodes with large $k^h$ being very small, the higher-order links still keep playing very crucial roles in steering localization for the larger eigenvalues. To get further insight into the role of higher-order links, we define the following quantities. Let $N_o(k^h > c)$ and $N_o(k^p > c)$ denote the set of nodes with $k^h > c$ and $k^p > c$, respectively. We are interested to find out the number of nodes which are common between these two sets, i.e., $N_o(k^h > c) \cap N_o(k^p > c)$ (Table I). It is evident from the table that total number of nodes in $N_o(k^h > c) \cap N_o(k^p > c)$ is less than 50% of set $N_o(k^h > c)$ for all $\gamma$ values and $c > 8$. Therefore, the impact of the higher-order links over the pairwise links in steering localization for larger eigenvalues is apparent more profoundly, which can be attributed to the increase in the $\langle k^p \rangle$ value with the increase in $\gamma$, whereas $\langle k^h \rangle = 3$ taking a constant value. Thus, $k^h(\lambda) \gg \langle k^h \rangle$ for the case of large eigenvalues for all $\gamma$ values. On the contrary, although the largest pairwise degree $k^p_{\max}$ experiences an increase with the increase in $\gamma$, at the same time $\langle k^p \rangle$ also increases, and, hence, $k^p(\lambda)$ does not deviate much from the pairwise average degree ($\langle k^p \rangle$) as compared to the deviation experienced by $k^h(\lambda)$ from higher-order average degree ($\langle k^p \rangle$). Mathematically, we can write $k^h(\lambda) - \langle k^h \rangle > k^p(\lambda) - \langle k^p \rangle$ for larger eigenvalues.

TABLE I. Number of nodes common between sets $N_o(k^h)$ and $N_o(k^p)$. For $N = 2000$ and 40 random realizations.

| | $\gamma = 3$ | $\gamma = 5$ | $\gamma = 7.5$ |
|---|---|---|---|
| $N_o(k^h > 8)$ | 3227 | 3212 | 3193 |
| $N_o(k^h > 12)$ | 585 | 582 | 611 |
| $N_o(k^h > 16)$ | 78 | 93 | 82 |
| $N_o(k^h > 20)$ | 10 | 7 | 13 |
| $N_o(k^p > 8)$ | 31509 | 69698 | 70494 |
| $N_o(k^p > 12)$ | 3418 | 582 | 79400 |
| $N_o(k^p > 16)$ | 125 | 6698 | 428561 |
| $N_o(k^p > 20)$ | 2 | 508 | 14487 |
| $N_o(k^h > 8) \cap N_o(k^p > 8)$ | 1286 | 2806 | 3168 |
| $N_o(k^h > 12) \cap N_o(k^p > 12)$ | 31 | 237 | 532 |
| $N_o(k^h > 16) \cap N_o(k^p > 16)$ | 0 | 7 | 46 |
| $N_o(k^h > 20) \cap N_o(k^p > 20)$ | 0 | 0 | 1 |

So far, by using $k^h(\lambda)$ and $k^p(\lambda)$, we have discussed the localization properties of the eigenvectors. Particularly, we have demonstrated that eigenvectors are localized on the nodes having the degree abnormally high or low either with respect to $\langle k^h \rangle$ or $\langle k^p \rangle$. Also, $k^h(\lambda)$ and $k^p(\lambda)$ come in the good approximation with $\hat{k}^h(\lambda)$ and $\hat{k}^p(\lambda)$, respectively. However, it is also important to scrutinize other eigenvector components to achieve the holistic idea of the localization. For this, we calculate the absolute value of the eigenvector components $|x_i|$, the higher-order degree of the corresponding node $k_i^h$, the pairwise degree $k_i^p$, and average them over $\lambda$ and $\lambda \pm d\lambda$

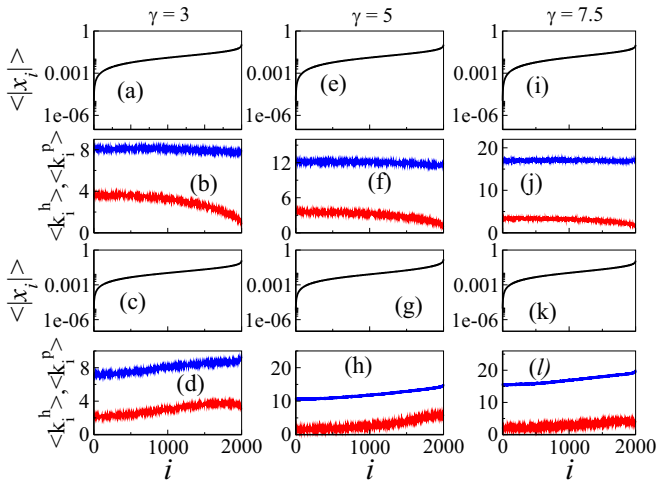


FIG. 7. $\langle|x_i|\rangle$ (black), $\langle k_i^h\rangle$ (red), and $\langle k_i^p\rangle$ (blue) against index $i$ for $\lambda$ belonging to the delocalized region. (a) and (b) $\lambda \approx 8.5$, (c) and (d) $\lambda \approx 14$, (e) and (f) $\lambda \approx 12.5$, (g) and (h) $\lambda \approx 23.5$, (i) and (j) $\lambda \approx 18$, and (k) and (l) $\lambda \approx 26$. The size of the hypergraph, $N = 2000$, and $M^h = 500$ remains fixed for all $\gamma$ values with 40 random realizations.

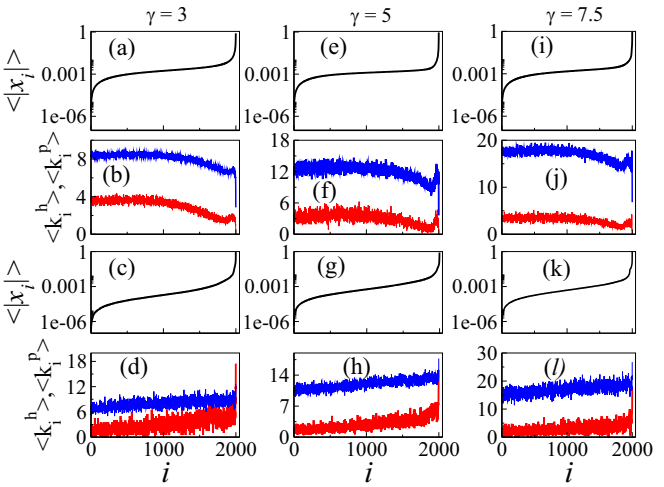


FIG. 8. $\langle|x_i|\rangle$ (black), $\langle k_i^h\rangle$ (red), and $\langle k_i^p\rangle$ (blue) against index $i$ for $\lambda$ belonging to the localized region. (a) and (b) $\lambda \approx 2$, (c) and (d) $\lambda \approx 33$, (e) and (f) $\lambda \approx 3$, (g) and (h) $\lambda \approx 36$, (i) and (j) $\lambda \approx 5$, and (k) and (l) $\lambda \approx 46$. The size of the hypergraphs $N = 2000$, and $M^h = 500$ remain fixed for all $\gamma$ values with 40 random realizations.

denoted by $\langle|x_i|\rangle$, $\langle k_i^h\rangle$, and $\langle k_i^p\rangle$. We consider different regions of the eigenvalue spectrum to calculate $\langle|x_i|\rangle$, $\langle k_i^h\rangle$, and $\langle k_i^p\rangle$. For the delocalized region, we consider the $\lambda$ values where $k^h(\lambda)$ intersects with $\hat{k}^h(\lambda)$, and $k^p(\lambda)$ intersects with $\hat{k}^h(\lambda)$. For the localized region, we consider $\lambda$ from the extremal eigenvalues, i.e., smaller and larger eigenvalues. Figure 7 presents the results for $\langle|x_i|\rangle$ arranged in an increasing order, and corresponding $\langle k_i^h\rangle$ and $\langle k_i^p\rangle$ for two $\lambda$ values belonging to the delocalized region for various $\gamma$ values. It is clearly visible that $\max(\langle|x_i|\rangle) \ll 1$ and most of the $\langle|x_i|\rangle$ are on the order of $10^{-2}$ and $10^{-3}$, respectively. It becomes more interesting to look at the behavior of $\langle k_i^h\rangle$ and $\langle k_i^p\rangle$. Both $\langle k_i^h\rangle$ and $\langle k_i^p\rangle$ remain constant to values, which are around $\langle k^h\rangle$ and $\langle k^p\rangle$, respectively, and, thus, validating the earlier results. Furthermore, Fig. 8 plots $\langle|x_i|\rangle$, $\langle k_i^h\rangle$, and $\langle k_i^p\rangle$ for $\lambda$ belonging to the localized region. It is apparent from that $(\max\langle|x_i|\rangle) \to 1$, and only a few entries are on the order of $10^{-1}$ depicting the localized nature of the eigenvectors. Furthermore, for smaller eigenvalues, $\langle k_i^h\rangle$ remains fixed to the values lying in the close vicinity to $\langle k^h\rangle \approx 3 \pm 2$ for all $i$'s. However, $\langle k_i^p\rangle$ deviates from $\langle k^p\rangle$ and dips down to a value which is lower than $\langle k^p\rangle$ for the node contributing maximum in $\langle|x_i|\rangle$. For the larger eigenvalues, $\langle k_i^h\rangle$ remains constant at around $\langle k^h\rangle$ for the nodes contributing minimal in $\langle|x_i|\rangle$, and takes value much larger than $\langle k^h\rangle$ for the nodes contributing maximal in $\langle|x_i|\rangle$. On the other hand, $\langle k_i^p\rangle$ always keeps oscillating around $\langle k^p\rangle$ for all $i$'s, and manifests a little deviation for $\langle k^p\rangle$ for large $i$. The above observations validate the earlier obtained result that localization at smaller eigenvalues is instigated by the pairwise links with higher-order links playing a dominant role in inducing localization for larger eigenvalues.

We emphasize that the results presented here are robust against the changes in the hypergraph parameters. The Supplemental Material [48] consists of the results for two other values of $M^h = 1000$ and 2000. The behavior of eigenvector localization is similar to that discussed here for $M^h = 500$. Additionally, we consider one more size of the hyperedges, i.e., $d = 4$, and the results manifest good agreements with those of $d = 3$.

*Localization properties of the conventional Laplacian.* Let us now discuss localization behavior of the eigenvectors for the conventional Laplacian matrices. As mentioned earlier, we consider $L^H$ instead of $L$ in our analysis. Unlike the conventional Laplacian ($L$), $L^H$ considers both the number and the size of hyperedges incident on the nodes and, thus, incorporates the higher-order structures completely. Here,

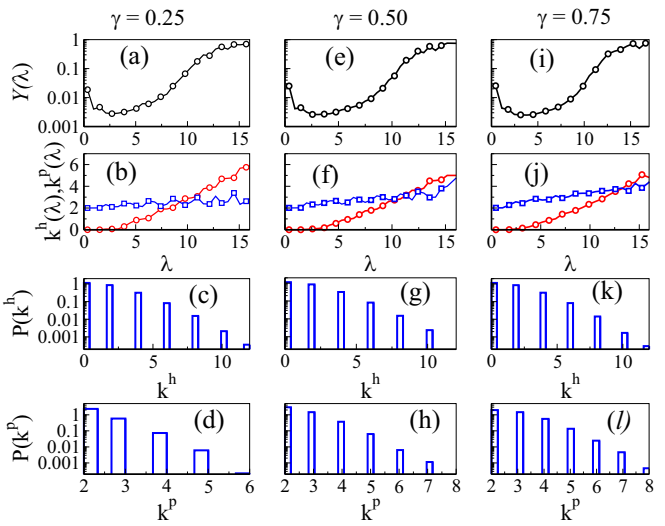


FIG. 9. Average IPR $[Y_{x_j}(\lambda)]$ (○), $k^h(\lambda)$ (○), and $k^p(\lambda)$ (□) against $\lambda$ for various $\gamma < 1$'s of the conventional Laplacian. The corresponding higher-order and pairwise degree distributions are also plotted in the last two rows. The size of the hypergraphs $N = 2000$ and $M^h = 500$ remain fixed for all $\gamma$ values with 40 random realizations.

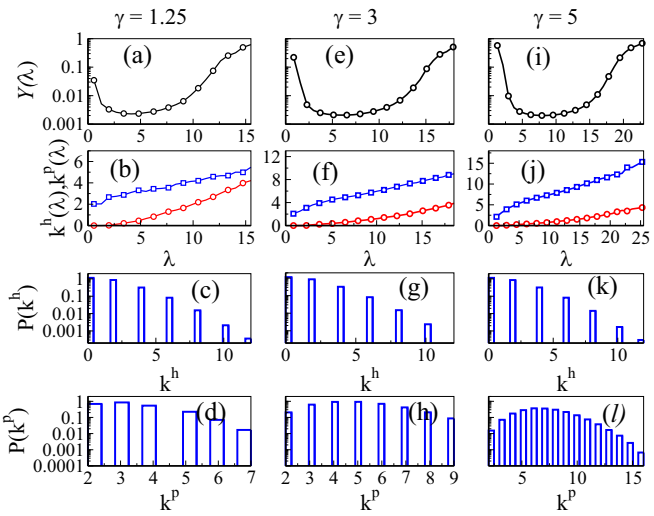


FIG. 10. Average IPR $[Y_{x_j}(\lambda)]$ (○), $k^h(\lambda)$ (○), and $k^p(\lambda)$ (□), for various $\gamma > 1$'s of the conventional Laplacian. The corresponding higher-order and pairwise degree distributions are also plotted in last two rows. The size of the hypergraphs $N = 2000$ and $M^h = 500$ remain fixed for all $\gamma$ values with 40 random realizations.

we present the results for the conventional Laplacian by calculating the same parameters as those used for $L^H$. Note that in the case of the conventional Laplacian $\gamma = \frac{M^p}{2M^h}$ since if a node is incident on one hyperedge, its degree will be increased by 2. From $\gamma < 1$, the localization behavior of the eigenvectors remains the same as that of $L^H$ (Fig. 9). However, for $\gamma > 1$, the localization behavior of the eigenvectors of $L$ displays a completely different behavior to that of $L^H$ (Fig. 10). The pairwise links play a more prominent role in steering localization for all $\gamma > 1$, and hyperlinks play a negligible effect. This may be due to the fact that the conventional Laplacian does not take into account the size of the hyperedges, and, thus, as pairwise links increase, it dominates the effect of hyperlinks on steering localization. Thus, the above observations indicate the importance of $L^H$ in capturing properties of higher-order interaction networks more accurately than the conventional Laplacian. Furthermore, this example provides insight about the importance of definition of Laplacian matrices, which depend on the physical system modeled on the hypergraph.

## VI. CONCLUSION

To conclude, we have investigated an interplay of the higher-order and the pairwise links in driving localization of the eigenvectors of hypergraphs. We find that the hypergraph eigenvectors are localized on the set of nodes having degrees either much higher or lower from the average degree, a result which is consistent with the earlier known result for the networks having only pairwise interactions. Furthermore, by defining a single parameter $\gamma$ which measures relative contribution of the pairwise and the higher-order links on a node, we show that pairwise links does not impart any impact on localization for $\gamma \leqslant 1$. For $\gamma > 1$ with an increase in $\gamma$, the degree of localization of the eigenvectors corresponding to the smaller eigenvalues increases. We show that role of higher-order links is not significant as compared to the pairwise links in inducing localization for smaller eigenvalues. This is due to the fact that average pairwise degree ($\langle k^p \rangle$) increases with the increase in $\gamma$, but the average higher-order degree ($\langle k^h \rangle = 3$) remains to a fixed value. Thus, the higher-order degree of the nodes contributing maximum in an eigenvector and averaged over $\lambda$ and $\lambda \pm d\lambda$ $[k^h(\lambda)]$ being small for lower eigenvalues cannot be substantially low as compared with $\langle k^h \rangle$ for all $\gamma$ values. On the contrary, the difference between the pairwise degree of a node contributing maximum in the eigenvector and and average pairwise degree ($\langle k^p \rangle$) start increasing with the increase in $\gamma$. Ergo, the pairwise links play a significant role in the eigenvector localization for smaller eigenvalues. Whereas, for larger eigenvalues, the higher-order links play a crucial role in instigating localization despite the fact that the number of nodes with the high value of higher-order degree ($k^h$) remains very small for all the $\gamma$ values. This can also be explained in a similar fashion which we adopted for the smaller eigenvalues. As $\langle k^h \rangle = 3$ remains fixed to a constant value for all $\gamma$ values, the difference between $k^h(\lambda)$ and $\langle k^h \rangle$ for larger eigenvalues always remain very high, whereas for the pairwise links though the largest pairwise degree $k^p_{\max}$ exhibits an increase with $\gamma$, there exists a simultaneous increase in $\langle k^p \rangle$. Therefore, the difference between $k^h(\lambda)$ and $\langle k^h \rangle$ is greater than the difference between $k^p(\lambda)$ and $\langle k^h \rangle$, i.e., $k^h(\lambda) - \langle k^h \rangle > k^p(\lambda) - \langle k^p \rangle$ for larger eigenvalues, which, in turn, indicates the importance of higher-order links on the localization for larger eigenvalues. The present paper can be extended to simplicial complexes in which higher-order degrees can be further decomposed into contributions attributed from different dimensions, such as triangles, tetrahedrons, and so on. Furthermore, investigating roles of higher-order and pairwise interactions, separately, on dynamics of random walkers is an interesting future direction.

## ACKNOWLEDGMENTS

S.J. gratefully acknowledges SERB Power Grant No. SPF/2021/000136. The work is supported by the computational facility received from the Department of Science and Technology (DST), Government of India under FIST scheme (Grant No. SR/FST/PSI-225/2016).

[1] R. Albert and A.-L. Barabási, Rev. Mod. Phys. **74**, 47 (2002).
[2] S. N. Dorogovtsev and J. F. Mendes, Adv. Phys. **51**, 1079 (2002).
[3] M. E. Newman, SIAM Rev. **45**, 167 (2003).
[4] C. Sarkar and S. Jalan, Chaos **28**, 102101 (2018).
[5] M. Salathé and J. H. Jones, PLOS Comput. Biol. **6**, e1000736 (2010); P. Holme, Phys. Rev. E **94**, 022305 (2016); M. D. Shirley and S. P. Rushton, Ecol. Complex **2**, 287 (2005).

[6] N. Masuda, M. A. Porter, and R. Lambiotte, Phys. Rep. **716-717**, 1 (2017).

[7] A. Arenas, A. Díaz-Guilera, J. Kurths, Y. Moreno, and C. Zhou, Phys. Rep. **469**, 93 (2008).

[8] F. Battiston, G. Cencetti, I. Iacopini, V. Latora, M. Lucas, A. Patania, J.-G. Young, and G. Petri, Phys. Rep. **874**, 1 (2020).

[9] G. Ghoshal, V. Zlatić, G. Caldarelli, and M. E. J. Newman, Phys. Rev. E **79**, 066118 (2009); E. Estrada and J. A. Rodriguez-Velazquez, Physica A: Stat. Mechanics Appli. **364**, 581 (2006); G. Ferraz de Arruda, M. Tizzani, and Y. Moreno, Commun. Phys. **4**, 24 (2021).

[10] O. T. Courtney and G. Bianconi, Phys. Rev. E **93**, 062311 (2016); S. Krishnagopal and G. Bianconi, *ibid.* **104**, 064303 (2021); J. J. Torres and G. Bianconi, J. Phys. Complexity **1**, 015002 (2020).

[11] S. Klamt, U.-U. Haus, and F. Theis, PLoS comput. Bio. **5**, e1000385 (2009); S. Feng, E. Heath, B. Jefferson, C. Joslyn, H. Kvinge, H. D. Mitchell, B. Praggastis, A. J. Eisfeld, A. C. Sims, L. B. Thackray *et al.*, BMC Bioinf. **22**, 287 (2021).

[12] V. Zlatić, G. Ghoshal, and G. Caldarelli, Phys. Rev. E **80**, 036118 (2009); J. Zhu, J. Zhu, S. Ghosh, W. Wu, and J. Yuan, IEEE Transactions on Network Science and Engineering **6**, 801 (2018).

[13] U. Alvarez-Rodriguez, F. Battiston, G. F. de Arruda, Y. Moreno, M. Perc, and V. Latora, Nat. Hum. Behav. **5**, 586 (2021); G. Burgio, J. T. Matamalas, S. Gómez, and A. Arenas, Entropy **22**, 744 (2020).

[14] B. Jhun, M. Jo, and B. Kahng, J. Stat. Mech. (2019) 123207.

[15] P. S. Chodrow, J. Complex Netw. **8**, cnaa018 (2020).

[16] Y. Wang, D. Chakrabarti, C. Wang, and C. Faloutsos, in *Proceedings of the 22nd International Symposium on Reliable Distributed Systems, 2003* (IEEE Computer Society, Los Alamitos, 2003), pp. 25–34.

[17] J. G. Restrepo, E. Ott, and B. R. Hunt, Phys. Rev. E **71**, 036151 (2005).

[18] A. Yadav and S. Jalan, Chaos **25**, 043110 (2015).

[19] S. Jalan, G. Zhu, and B. Li, Phys. Rev. E **84**, 046107 (2011).

[20] S. Jalan and J. N. Bandyopadhyay, Phys. Rev. E **76**, 046107 (2007).

[21] T. Raghav and S. Jalan, Physica A **586**, 126457 (2022).

[22] B. Mohar, Y. Alavi, G. Chartrand, and O. Oellermann, Graph theory, combinatorics, and applications **2**, 871 (1991), https://www.researchgate.net/profile/Ortrud-Oellermann/publication/233407318_The_Laplacian_spectrum_of_graphs/links/00b495251b10155235000000/The-Laplacian-spectrum-of-graphs.pdf.

[23] S. Bradde, F. Caccioli, L. DallAsta, and G. Bianconi, Phys. Rev. Lett. **104**, 218701 (2010); O. Mülken and A. Blumen, Phys. Rep. **502**, 37 (2011); R. Burioni and D. Cassi, Phys. Rev. Lett. **76**, 1091 (1996).

[24] R. Burioni, D. Cassi, A. Vezzani, Phys. Rev. E **60**, 1500 (1999).

[25] T. H. K. Hattori and H. Watanabe, Prog. Theor. Phys. Suppl. **92**, 108 (1987).

[26] M. Barahona and L. M. Pecora, Phys. Rev. Lett. **89**, 054101 (2002); L. M. Pecora and T. L. Carroll, *ibid.* **80**, 2109 (1998).

[27] I. Leyva, I. Sendiña-Nadal, J. A. Almendral, and M. A. F. Sanjuán, Phys. Rev. E **74**, 056112 (2006); A. Arenas, A. Diaz-Guilera, and C. J. Pérez-Vicente, Phys. Rev. Lett. **96**, 114102 (2006).

[28] P. Pradhan, C. Angeliya, and S. Jalan, Physica A **554**, 124169 (2020).

[29] S. Jalan and J. N. Bandyopadhyay, Physica A **387**, 667 (2008).

[30] A. V. Goltsev, S. N. Dorogovtsev, J. G. Oliveira, and J. F. F. Mendes, Phys. Rev. Lett. **109**, 128702 (2012).

[31] S. Suweis, J. Grilli, J. R. Banavar, S. Allesina, and A. Maritan, Nat. Commun. **6**, 10179 (2015).

[32] V. Plerou, P. Gopikrishnan, B. Rosenow, L. A. Nunes Amaral, and H. E. Stanley, Phys. Rev. Lett. **83**, 1471 (1999); F. Slanina and Z. Konopásek, Advances in Complex Systems **13**, 699 (2010).

[33] J. Moran and J.-P. Bouchaud, Phys. Rev. E **100**, 032307 (2019).

[34] S. Hata, H. Nakao, and A. S. Mikhailov, Sci. Rep. **4**, 3585 (2014); H. Nakao and A. S. Mikhailov, Nat. Phys. **6**, 544 (2010).

[35] T. Carletti, F. Battiston, G. Cencetti, and D. Fanelli, Phys. Rev. E **101**, 022308 (2020).

[36] T. Carletti, D. Fanelli, and R. Lambiotte, J. Phys. Complexity **2**, 015011 (2021).

[37] A. Krawiecki, Chaos, Solitons Fractals **65**, 44 (2014).

[38] R. Mulas, C. Kuehn, and J. Jost, Phys. Rev. E **101**, 062313 (2020).

[39] T. Carletti, D. Fanelli, and S. Nicoletti, J. Phys. Complexity **1**, 035006 (2020).

[40] G. F. de Arruda, G. Petri, and Y. Moreno, Phys. Rev. Res. **2**, 023032 (2020).

[41] D. Bollé, R. Heylen, and N. S. Skantzos, Phys. Rev. E **74**, 056111 (2006).

[42] M. E. J. Newman and D. J. Watts, Phys. Rev. E **60**, 7332 (1999).

[43] R. Monasson, Eur. Phys. J. B **12**, 555 (1999).

[44] A. Mishra, J. N. Bandyopadhyay, and S. Jalan, Chaos, Solitons Fractals **144**, 110745 (2021).

[45] F. Slanina, Phys. Rev. E **95**, 052149 (2017).

[46] C. Zhan, G. Chen, and L. F. Yeung, Physica A **389**, 1779 (2010).

[47] S. Hata and H. Nakao, Sci. Rep. **7**, 1121 (2017).

[48] See Supplemental Material at http://link.aps.org/supplemental/10.1103/PhysRevE.107.034311 for results for other hypergraph parameters.

[49] P. N. McGraw and M. Menzinger, Phys. Rev. E **77**, 031102 (2008).